RESEARCH ARTICLE

Axisymmetric diffusion kurtosis imaging with Rician bias correction: A simulation study

Jan Malte Oeschger[1] | **Karsten Tabelow[2]** | **Siawoosh Mohammadi[1,3]**

[1]Institute of Systems Neuroscience, University Medical Center Hamburg-Eppendorf, Hamburg, Germany

[2]Weierstrass Institute for Applied Analysis and Stochastics, Berlin, Germany

[3]Department of Neurophysics, Max Planck Institute for Human Cognitive and Brain Sciences, Leipzig, Germany

Correspondence
Jan Malte Oeschger, Institute of Systems Neuroscience, University Medical Center Hamburg-Eppendorf, Martinistraße 52, 20246 Hamburg, Germany.
Email: j.oeschger@uke.de

Correction added after online publication 12 December 2022. Due to a production error, the following changes were not incorporated before publication: The delta symbol in the paragraph preceding equation 3 is restored to δxy; one of the 'g vector' symbols of Figure 4 has been corrected; the author's name in the 'How to cite this article' information has been corrected.

Purpose: To compare the estimation accuracy of axisymmetric diffusion kurtosis imaging (DKI) and standard DKI in combination with Rician bias correction (RBC).

Methods: Axisymmetric DKI is more robust against noise-induced variation in the measured signal than standard DKI because of its reduced parameter space. However, its susceptibility to Rician noise bias at low signal-to-noise ratios (SNR) is unknown. Here, we investigate two main questions: first, does RBC improve estimation accuracy of axisymmetric DKI?; second, is estimation accuracy of axisymmetric DKI increased compared to standard DKI? Estimation accuracy was investigated on the five axisymmetric DKI tensor metrics (AxTM): the parallel and perpendicular diffusivity and kurtosis and mean of the kurtosis tensor, using a noise simulation study based on synthetic data of tissues with varying fiber alignment and in-vivo data focusing on white matter.

Results: RBC mainly increased accuracy for the parallel AxTM in tissues with highly to moderately aligned fibers. For the perpendicular AxTM, axisymmetric DKI without RBC performed slightly better than with RBC. However, the combination of axisymmetric DKI with RBC was the overall best performing algorithm across all five AxTM in white matter and axisymmetric DKI itself substantially improved accuracy in axisymmetric tissues with low fiber alignment.

Conclusion: Combining axisymmetric DKI with RBC facilitates accurate DKI parameter estimation at unprecedented low SNRs (≈ 15) in white matter, possibly making it a valuable tool for neuroscience and clinical research studies where scan time is a limited resource. The tools used here are available in the open-source ACID toolbox for SPM.

KEYWORDS
axisymmetric DKI, microscopic fiber alignment, noise, Rician bias correction, simulation

1 | INTRODUCTION

Diffusion weighted MRI is an in-vivo imaging modality used in neuroscience and clinical research. It is sensitive to changes in nervous tissues that, for example, go along with neurodegenerative diseases like epilepsy and multiple sclerosis.[1,2] Diffusion MRI measures the net diffusion of nuclear spins of hydrogen nuclei in water molecules that are omnipresent in nervous tissue.

Diffusion of water molecules within the microstructural tissue landscape can be arbitrarily complex. A data-efficient method that captures both standard Gaussian diffusion and more complex restricted diffusion processes (e.g., due to diffusion of water trapped in the cell-body of axons), is the recently introduced axisymmetric diffusion kurtosis imaging (DKI) framework.[3,4] Its data-efficiency stems from requiring only eight parameters due to assuming axisymmetrically distributed axons, instead of 22 parameters like standard DKI.[5] This is likely a reasonable assumption in major white matter fiber bundles.[3] Furthermore, this is expected to make axisymmetric DKI less susceptible to the noise induced variation of the acquired diffusion MRI signals.

Noise in MRI images introduces a random variation into the measured diffusion signals and a bias for the estimated DKI parameters when the signal-to-noise-ratio[6] (SNR) is low. This bias is known as the "Rician noise bias"[7-9] and becomes more severe, the lower the SNR is. Diffusion MRI is prone to a low SNR because it generates image contrast from additional spin dephasing associated with water mobility leading to a signal attenuation. DKI is even more susceptible to the Rician noise bias compared to conventional diffusion tensor imaging, since estimating the DKI parameters requires multiple diffusion shells including higher diffusion weighting, lowering the SNR. This increases the demand for effective Rician bias correction (RBC) schemes[10,11] in DKI. Currently, it is unclear whether fitting the axisymmetric DKI framework with its reduced parameter space is better suited for parameter estimation from noisy diffusion MRI data than standard DKI and if its susceptibility to Rician noise bias is reduced.

The effect of the Rician noise bias on the fractional anisotropy (FA), mean diffusivity (MD), mean kurtosis (MK), diffusion tensor elements and diffusion kurtosis tensor elements was shown to be mitigated by using RBC in standard DKI.[10,12-14] Of these parameters only the mean kurtosis provides similar contrast as the mean of the kurtosis tensor $\overline{W}$ and thus can be considered part of the axisymmetric DKI tensor metrics (AxTM). The AxTM are the parallel and perpendicular diffusivities ($D_\parallel$ and $D_\perp$), the parallel and perpendicular kurtosis and mean of the kurtosis tensor ($W_\parallel$, $W_\perp$, and $\overline{W}$). Here, parallel and perpendicular are in reference to the axis of symmetry. The

TABLE 1 AxTM and standard diffusion kurtosis imaging (DKI) tensor metrics with which they are calculated

Axisymmetric DKI tensor metric (AxTM)	Corresponding standard DKI tensor metrics
$D_\parallel$	1: λ_1
$D_\perp$	2: λ_2, λ_3
$W_\parallel$	1: W_{1111}
$W_\perp$	3: $W_{2222}, W_{3333}, W_{2233}$
$\overline{W}$	6: $W_{1111}, W_{2222}, W_{3333},$ $W_{1122}, W_{1133}, W_{2233}$

Notes: The numbers show how many standard DKI tensor metrics are needed to compute the AxTM. λ refers to the eigenvalues of the diffusion tensor, W refers to the components of the kurtosis tensor.

axisymmetric DKI framework contains three additional parameters, the two angles of the unit vector pointing along the axis of symmetry, and the nondiffusion-weighted signal ($b = 0$).

The AxTM can be estimated based on standard DKI and computed as aggregates from its 22 tensor metrics or directly with axisymmetric DKI (see Table 1). The AxTM are of particular interest for neuroscience and clinical research[15-17] because they are invariant against coordinate transformations and describe free and restricted diffusion within nervous tissue. Furthermore, the AxTM can be directly related to the tissue microstructure[18,19] via the axon water fraction, axon dispersion, and three diffusivities associated with the intra- and extra-axonal space.

It was shown empirically,[13] that RBC will impact the estimation of the parallel and perpendicular AxTM differently. It was speculated that the parallel and perpendicular AxTM are associated with different levels of water mobility and consequently different levels of SNR. Furthermore, another open question is the influence of fiber alignment on the effectiveness of RBC. It can be expected that the degree of fiber alignment within a white matter MRI voxel affects water mobility and thereby also the effectiveness of RBC.

In this work two main questions are investigated: First, we investigate whether RBC also increases the estimation accuracy of axisymmetric DKI. Second, we investigate whether the estimation accuracy is improved by using axisymmetric DKI as compared to standard DKI. Moreover, we investigate whether the performance of RBC depends on tissue fibre alignment and investigate differences in effectiveness for the parallel and perpendicular AxTM. To study these questions, we simulated two classes of datasets: the "synthetic dataset" is based on three sets of synthetic AxTM describing tissues with varying degrees of fiber alignment which allows us to assess AxTM estimation accuracy as a function of fiber alignment; the "in-vivo white matter dataset"

and "`in-vivo gray matter dataset`" are based on invivo measurements of white matter tissue fiber tracts with a high to moderate fiber alignment (`in-vivo white matter dataset`) or typical gray matter areas (`in-vivo gray matter dataset`) which allows us to study AxTM estimation accuracy under realistic, in-vivo conditions. In both studies, axisymmetric DKI and standard DKI (with and without RBC) were used to obtain estimates of the five AxTM that could then be compared to the ground truth.

2 | METHODS

2.1 | Standard DKI signal representation

For a given diffusion weighting b and diffusion gradient $\vec{g} = (g_1, g_2, g_3)^\mathsf{T}$, the noise-free DKI signal $\tilde{S}_{b,\vec{g}}$ can be represented as in:[5,20]

$$\tilde{S}_{b,\vec{g}}(\tilde{S}_0, D, W) = \tilde{S}_0 \exp\left[-bD + \frac{b^2}{6}\left(\frac{\mathrm{Tr}(D)}{3}\right)^2 W\right] \quad (1a)$$

$$D = \sum_{i,j=1}^{3} g_i g_j D_{ij} \quad (1b)$$

$$W = \sum_{i,j,k,l=1}^{3} g_i g_j g_k g_l W_{ijkl} \quad (1c)$$

where D_{ij} are the diffusion tensor entries, W_{ijkl} are the kurtosis tensor entries and $\tilde{S}_0$ is the non-diffusion-weighted signal ($b = 0\frac{\mathrm{s}}{\mathrm{mm}^2}$).

From the tensors D and W, the AxTM can be directly computed: $D_\| = \lambda_1$ where λ_1 is the first eigenvalue of the diffusion tensor D, $D_\perp = (\lambda_2 + \lambda_3)/2$.

$W_\|$ and $W_\perp$ can be computed from the fitted W tensor according to formulas 11 and 12 from:[3] $W_\| = W(\nu_1) = W_{1111}$, where ν_1 is the first eigenvector of the corresponding diffusion tensor and $W_\perp = 3/8(W_{2222} + W_{3333} + 2W_{2233})$. $\overline{W}$ can be computed according to equation 10 from:[21] $\overline{W} = 1/5(W_{1111} + W_{2222} + W_{3333} + 2W_{1122} + 2W_{1133} + 2W_{2233})$ (in:[21] 1 = x, 2 = y, 3 = z).

2.2 | Axisymmetric DKI

Axisymmetric DKI[3] assumes symmetric diffusion around an axis of symmetry $\vec{c}$ inside an imaging voxel. Mathematically, this assumption leads to axisymmetric diffusion and kurtosis tensors with a drastically reduced number of independent tensor parameters compared to standard DKI (from 15 to 3 parameters for the kurtosis tensor and from 6 to 2 parameters for the diffusion tensor). In addition to the five AxTM, axisymmetric DKI contains two parameters for the axis of symmetry (inclination and azimuth). The symmetry assumptions are likely a reasonable approximation to diffusion in major white matter fiber bundles[3] due to their structural organization, which is why the focus of this study is white matter.

With the axis of symmetry $\vec{c}$ parameterized by the inclination θ and azimuth ϕ: $\vec{c} = (\sin\theta\cos\phi, \sin\theta\sin\phi, \cos\theta)^\mathsf{T}$, the diffusion and kurtosis tensors can be determined according to:[3]

$$D = D_\|\mathbf{I} + (D_\| - D_\perp)\vec{c}\,\vec{c}^T, \quad (2)$$

and

$$W = \frac{1}{2}(10W_\perp + 5W_\| - 15\overline{W})\mathbf{P} + W_\perp\Lambda$$
$$+ \frac{3}{2}(5\overline{W} - W_\| - 4W_\perp)\mathbf{Q},$$

where $\Omega = \{D_\|, D_\perp, W_\|, W_\perp, \overline{W}, \tilde{S}_0, \theta, \phi\}$ are the eight framework's parameters ($\tilde{S}_0$ is the nondiffusion-weighted signal) and $\mathbf{I}$ is the three-dimensional identity matrix. The tensors $\mathbf{P}, \Lambda$, and $\mathbf{Q}$ can be computed with the Kronecker delta δ_{xy} and the components of the axis of symmetry c_x ($x, y \in 1, 2, 3$) as: $\mathbf{P}_{ijkl} = c_i c_j c_k c_l$, $\mathbf{Q}_{ijkl} = (1/6)(c_i c_j \delta_{kl} + c_i c_k \delta_{jl} + c_i c_l \delta_{jk} + c_j c_k \delta_{il} + c_j c_l \delta_{ik} + c_k c_l \delta_{ij})$ and $\Lambda_{ijkl} = (1/3)(\delta_{ij}\delta_{kl} + \delta_{ik}\delta_{jl} + \delta_{il}\delta_{jk})$.[3] The associated noise-free signal $\tilde{S}_{b,\vec{g}}(\Omega)$ can then be computed based upon the axisymmetric tensors:[22]

$$\tilde{S}_{b,\vec{g}}(\Omega) = \tilde{S}_0 \exp(-B_{ij}D_{ij} + \frac{1}{6}\overline{D}^2 B_{ij}B_{kl}W_{ijkl}), \quad (3)$$

where

$$B_{ij}D_{ij} = \mathrm{Tr}(B)D_\perp + (D_\| - D_\perp)\vec{c}^T B\vec{c}, \quad (4)$$

and

$$B_{ij}B_{kl}W_{ijkl} = \frac{1}{2}(10W_\perp + 5W_\| - 15\overline{W})(\vec{c}^T B\vec{c})^2$$
$$+ \frac{1}{2}(5\overline{W} - W_\| - 4W_\perp)(\vec{c}^T B\vec{c}\mathrm{Tr}(B)$$
$$+ 2\vec{c}^T BB\vec{c}) + \frac{W_\perp}{3}(Tr(B)^2 + 2\mathrm{Tr}(B \otimes B)),$$

with $B = b\begin{pmatrix} g_x^2 & g_x g_y & g_x g_z \\ g_x g_y & g_y^2 & g_y g_z \\ g_x g_z & g_y g_z & g_z^2 \end{pmatrix}$.

The AxTM can be computed from the standard DKI tensor metrics assuming axial-symmetry, see Section 2.1. Table 1 shows the AxTM and the standard DKI tensor metrics needed to compute them. Figure 1 shows the five AxTM obtained with the axisymmetric DKI fit without RBC, available in the open source ACID toolbox for SPM.
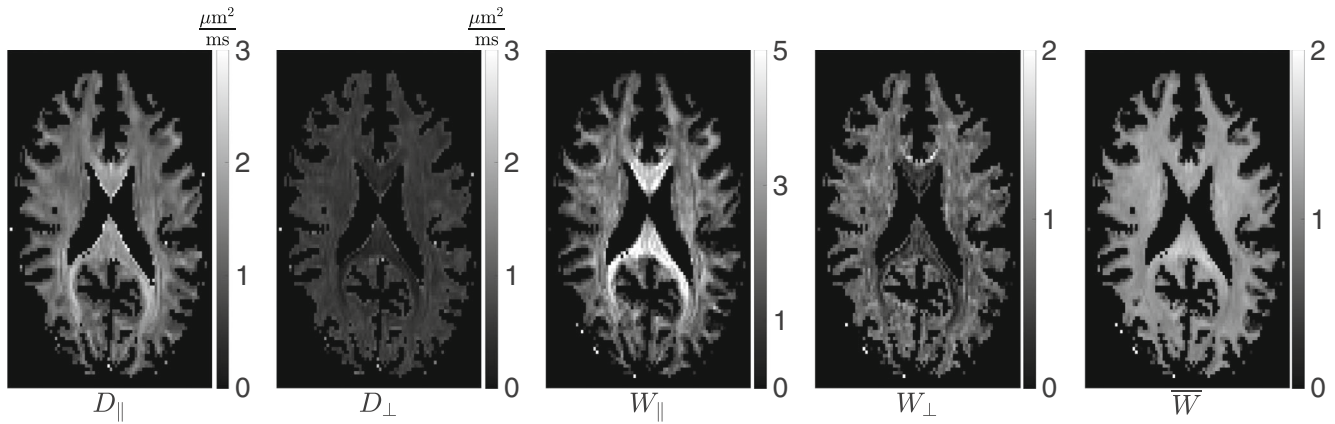
FIGURE 1 Axisymmetric diffusion kurtosis imaging (DKI) tensor metric (AxTM) results in white matter. The AxTM are the parallel and perpendicular diffusivity and kurtosis and the mean of the kurtosis tensor. The shown maps were obtained with the axisymmetric DKI fit available in the open source ACID toolbox for SPM that was used in this work. The AxTM were estimated from the in-vivo measurement used for the `in-vivo white matter (and gray matter) dataset` (Figure 3).

2.3 │ Parameter estimation and the Rician noise bias

A detailed version of this section can be found in Section S1.1 of Appendix S1.

Often standard DKI or axisymmetric DKI parameters are estimated using the acquired magnitude signals $S_{b,\vec{g}}$ and Equation (1a) or (3) with the least-squares approach[23-25] (found fit results are denoted with a hat, i.e., $\hat{S}_0, \hat{D}, \hat{W}$):

$$(\hat{S}_0, \hat{D}, \hat{W}) = \underset{\tilde{S}_0, D, W}{\mathrm{argmin}} \sum_i (S_{b,\vec{g}_i} - \tilde{S}_{b,\vec{g}_i}(\tilde{S}_0, D, W))^2. \quad (5)$$

However, this can be biased by the Rician noise bias. The severity of the Rician noise bias in the estimated parameters depends on the SNR:[26] the lower the SNR, the larger the bias. For RBC, we rely on an approach outlined in[26] that uses the expectation value $\mathbf{E}(S_{b,\vec{g}})$ of the noisy composite magnitude dMRI signal. The probability density function of $S_{b,\vec{g}}$ is a noncentral χ distribution whose expectation value $\mathbf{E}(S_{b,\vec{g}})$ is given by:[26]

$$\mathbf{E}(S_{b,\vec{g}}) = \mathbf{E}(\tilde{S}_{b,\vec{g}}(\tilde{S}_0, D, W), \sigma)$$
$$= \sigma\sqrt{\frac{\pi}{2}} \cdot \mathbf{L}_{1/2}^{(L-1)}\left(\frac{\tilde{S}_{b,\vec{g}}(\tilde{S}_0, D, W)^2}{2\sigma^2}\right), \quad (6)$$

where $\mathbf{L}_{1/2}^{(L-1)}(x) = \Gamma(L + 1/2)/(\Gamma(3/2)\Gamma(L))\mathbf{M}(-1/2, L, x)$ is the generalized Laguerre polynomial which can be expressed using a confluent hypergeometric function $\mathbf{M}$, the Gamma function Γ and the number of receiver coils L. Following,[26] we implemented a time-efficient Gauss Newton fitting algorithm[27] (see Section S1.2 of Appendix S1) that, unlike Equation (5), accounts for Rician noise

in magnitude dMRI data by solving the optimization problem:

$$(\hat{S}_0, \hat{D}, \hat{W}) = \underset{\tilde{S}_0, D, W}{\mathrm{argmin}} \sum_i (S_{b,\vec{g}_i} - \mathbf{E}(\tilde{S}_{b,\vec{g}_i}(\tilde{S}_0, D, W), \sigma))^2. \quad (7)$$

Estimating parameters this way is referred to as "quasi-likelihood" estimation and is denoted as "RBC ON" in this paper.

Rician bias corrected, standard DKI or axisymmetric DKI parameter estimation can be done by using Equation (1a) or Equation (3) to compute the noise-free signal predictions $\tilde{S}_{b,\vec{g}}$, then using Equation (6) to compute $\mathbf{E}(\tilde{S}_{b,\vec{g}}(\tilde{S}_0, D, W), \sigma)$ and finally minimize Equation (7) to estimate the framework parameters $(\hat{S}_0, \hat{D}, \hat{W})$ for standard DKI or Ω for axisymmetric DKI.

2.4 │ Simulation study: datasets and overview

A detailed version of this section can be found in Section S1.3 of Appendix S1.

We assessed estimation accuracy of the five AxTM as a function of the SNR in a simulation study with two classes of datasets, see Figure 2. The first class, the "`synthetic dataset`," consisted of three synthetic voxels with varying fiber alignment (defined in Reference 28). The other class of datasets was based on an in-vivo measurement and consisted of either 12 major white matter fiber tract voxels ("`in-vivo white matter dataset`") or 12 voxels from typical gray matter areas ("`in-vivo gray matter dataset`"). For all datasets, magnitude diffusion MRI data were simulated for varying SNRs and fitted
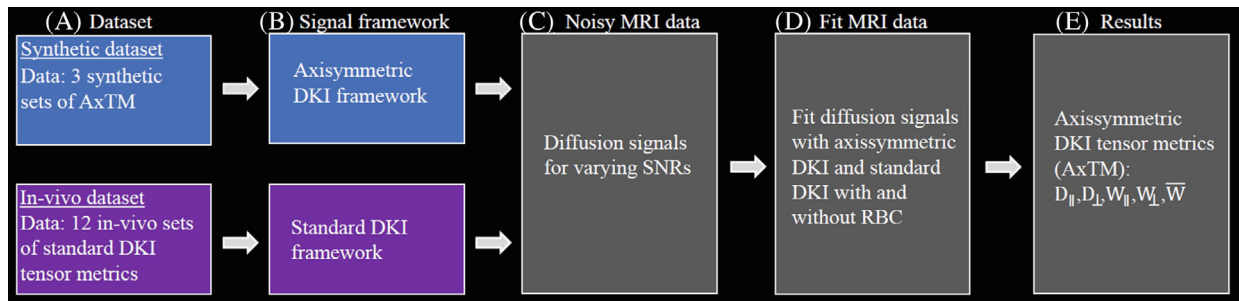
FIGURE 2 Scheme of the simulation study. Simulations were performed in 5 steps: (A) choice of datasets, (B) signal framework used for simulation, (C) diffusion signal simulation and contamination with noise, (D) parameter estimation, and (E) results. Note that both simulation studies only differed in (A) and (B) but were identical in the following procedures. (A) the `synthetic dataset` consisted of 3×5 sets of axisymmetric diffusion kurtosis imaging (DKI) tensor metric (AxTM) (Table S1) while the `in-vivo dataset` (either white matter or gray matter) consisted of 12×22 standard DKI tensor metrics (Table S2 lists the white matter data while Table S4 lists the gray matter data). (B) The DKI signal framework used for diffusion signal simulation. (C) Diffusion signal data were contaminated with 2500 Rician noise samples for each signal-to-noise ratio, SNR = [1, 2, 3...200]. (D) Simulated diffusion data were fitted with axisymmetric DKI and standard DKI with and without Rician bias correction in both simulation studies for each of the 2500 noise samples. (E) The axisymmetric DKI tensor metrics (AxTM): $D_{\parallel}, D_{\perp}, W_{\parallel}, W_{\perp}$ and $\overline{W}$ were calculated for standard DKI (for axisymmetric DKI they were directly estimated), averaged across the 2500 noise samples per SNR and finally compared to the ground truth.

with standard DKI and axisymmetric DKI, with and without RBC (as described in Section 2.3) to obtain estimates of the five AxTM. Accuracy of the obtained AxTM estimates were evaluated as the absolute value of the mean percentage error (A-MPE):

$$\text{A-MPE} = 100 \cdot \frac{|\text{GT} - \overline{\text{FitResults}(\text{SNR})}|}{\text{GT}}. \quad (8)$$

Here GT refers to the ground truth and $\overline{\text{FitResults}}$ refers to the average of the fit results over the noise samples. We evaluated the accuracy of the AxTM estimates for each estimation method by looking for the SNR after which the A-MPE was smaller 5%, which was considered an acceptable error in a trade-off between estimation accuracy and SNR requirement. As a summary to compare each method, we looked at the maximum SNR needed across the five AxTM for which A-MPE consistently < 5% for all AxTM ("Maximum" column in Figure 6).

2.4.1 | Datasets

The `synthetic dataset` consisted of three synthetic sets of AxTM (from Reference 28) describing three voxels with varying fiber alignment, one with fibers with low alignment ("LA", FA = 0.067), one with fibers with moderate alignment ("MA", FA = 0.24) and one with highly aligned fibers ("HA", FA = 0.86). The AxTM of the three synthetic voxels are summarized in Table S1. Figure 4 shows two areas of typical brain regions in a map of the mean of the kurtosis tensor $\overline{W}$ where LA and HA voxels

can be found and the corresponding idealized fiber stick model.

The `in-vivo white matter dataset` consists of 12 voxels extracted from four major white matter tracts (three voxels from each of the four fiber tracts, see Figure 3) from an in-vivo brain measurement (SNR = 23.4) of a healthy volunteer, details on the DWI acquisition sequence can be found in Section S1.3 of Appendix S1 . The 12 voxels were extracted from the in-vivo measurement by fitting the standard DKI framework in 12 white matter voxels of the acquired in-vivo DWI magnitude images to get the corresponding 22 standard DKI tensor metrics, the derived data are therefore referred to as "in-vivo white matter". Three voxels each with HA to MA (defined through the FA threshold FA $\geq$ 0.4 [29]) were extracted, see Figure 3 . The selected voxels differ from the synthetic voxels in that here only HA and MA voxels were selected. The extracted white matter standard DKI tensor metrics (Table S2) and corresponding AxTM (Table S3) are documented in the Appendix S1 .

The `in-vivo gray matter dataset` was produced according to the same procedure used for the `in-vivo white matter dataset` , only that the voxels were selected from typical gray matter areas. The extracted gray matter standard DKI tensor metrics (Table S4) and corresponding AxTM (Table S5) are documented in the Appendix S1 . Since white matter is the focus of this article, details and results of the `in-vivo gray matter dataset` can be found in Section S1.5 of Appendix S1 .

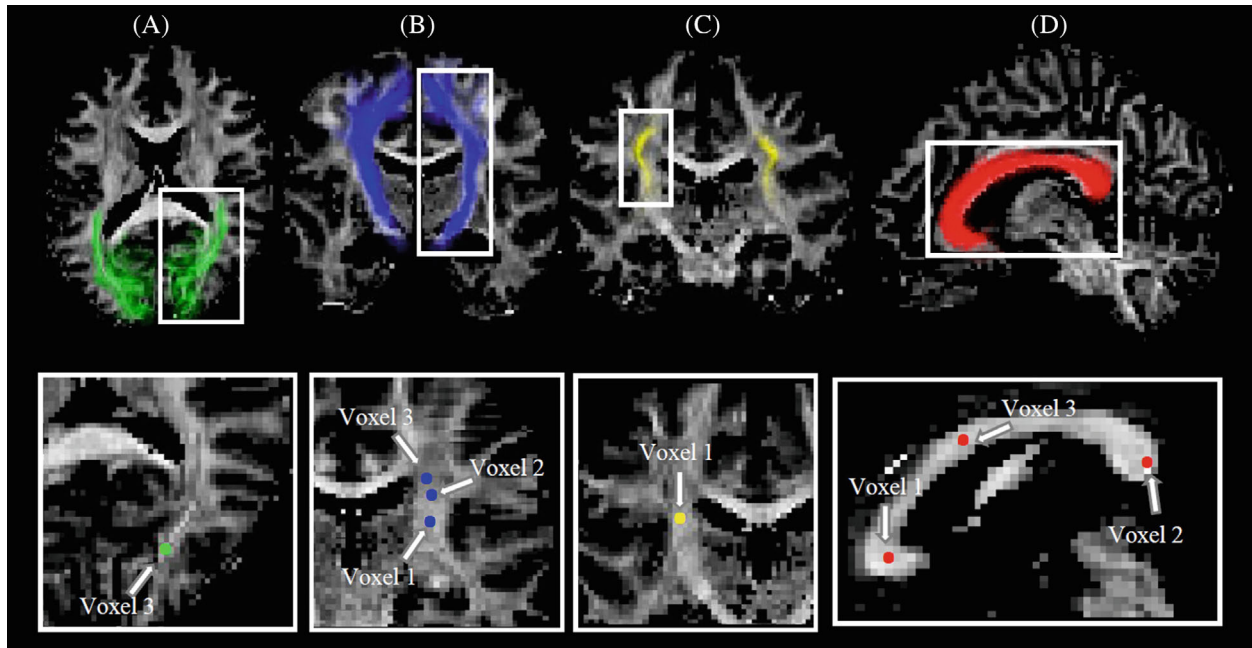The in-vivo dMRI data used for this study were acquired with the help of a human research participant.

FIGURE 3 Selection of voxels of the `in-vivo white matter dataset`: The four white matter fiber pathways within which voxels were selected and used as a basis for the `in-vivo white matter dataset`. Top: (A) Optic radiation (or), (B) cortico spinal tract (ct), (C) superior longitudinal fasciculus (slf) and (D) callosum body (cb) in a fractional anisotropy (FA) map of a healthy human brain. The fiber pathways were identified with the coregistered Jülich fiber atlas.[30] Bottom: Voxels in the fiber pathways used for the `in-vivo white matter dataset`. In each fiber pathway, three voxels were chosen for the `in-vivo white matter dataset` (for slf an or only one is shown here because the three chosen voxels were not in the same slice).

The participant provided written informed consent and was compensated for its participation. The local ethics committees at University Medical Center Hamburg-Eppendorf approved the study (PV5141).

2.4.2 | Signal framework used for simulation

The three synthetic voxels of AxTM were simulated with the axisymmetric DKI framework to first obtain noise-free diffusion MRI signals $\tilde{S}_{noise-free}$. The 12 in-vivo white matter and gray matter voxels were simulated with the standard DKI framework to first obtain noise-free diffusion MRI signals $\tilde{S}_{noise-free}$.

2.4.3 | Contamination with noise

For both the `synthetic` and the `in-vivo dataset` (white matter or gray matter), the noise-free diffusion MRI signals $\tilde{S}_{noise-free}$ were contaminated with noise for SNRs [1, 2, 3...200] and magnitude signals S_{cont} were computed. The noisy magnitude signals were computed according to $S_{cont} = |\tilde{S}_{noise-free} + \alpha + \beta i|$, where $\alpha, \beta \in \mathcal{N}(0, \sigma)$ are drawn from a zero mean Gaussian with SD σ, yielding different SNR = $\sqrt{2}S_0/\sigma$ (for one receiver coil) for a given $S_0 = 1$.

2.4.4 | Estimating the five AxTM

Both, the simulated signals S_{cont} from the `synthetic` and the `in-vivo dataset` were fitted with axisymmetric DKI and standard DKI, with and without RBC (Section 2.3) to obtain estimates of the AxTM whose accuracy could then be investigated as a function of SNR.

2.5 | Diffusion signal profiles influenced by fiber alignment

To further elucidate differences between tissues with different levels of fiber alignment, angular signal profiles under the influence of noise were studied for the three voxels of the `synthetic dataset`. Noise-free and noise-contaminated signals have been simulated (SNR = 20). The simulated signal's mean and SD could then be plotted as a function of angle ψ (in degree) between diffusion gradient $\vec{g}$ and axis of symmetry $\vec{c}$. For a graphical representation of angle ψ, see Figure 4.

3 | RESULTS

First, the results of the diffusion signal profiles in voxels with different levels of fiber alignments (Section 3.1) are

FIGURE 4 Model of fiber alignment in characteristic areas of the brain. Bottom: in-vivo map of the mean of the kurtosis tensor $\overline{W}$ with a typical area where fibers with low alignment (LA) are found and a typical area where highly aligned fibers (HA) are found. Top: the corresponding golden and red sticks depict an idealized model of the underlying fiber arrangement, the white dashed line indicates the axis of symmetry $\vec{c}$, the green dashed line indicates the diffusion gradient direction $\vec{g}$, ψ is the angle between $\vec{g}$ and $\vec{c}$.
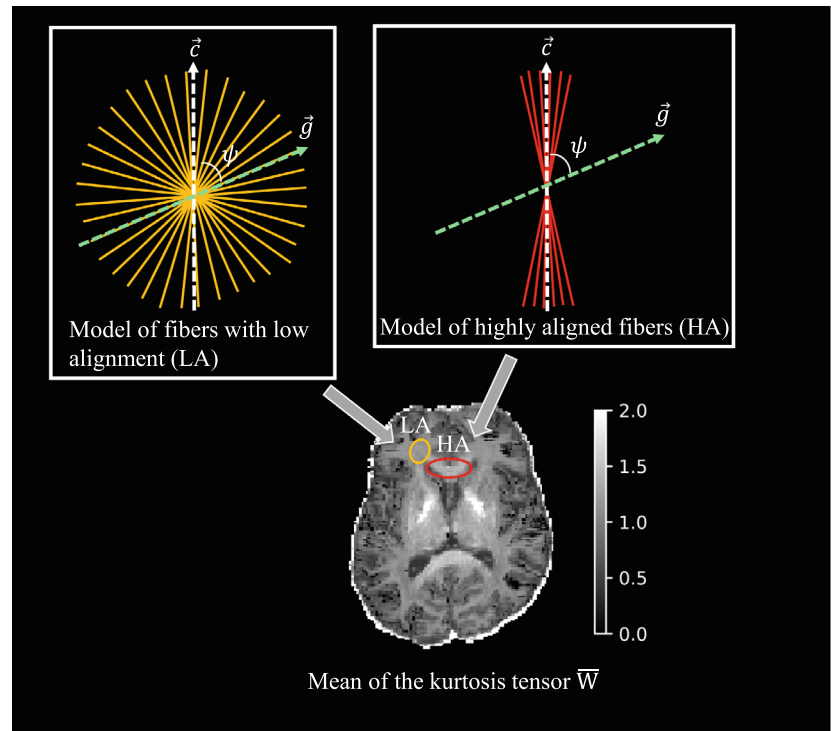
shown because these not only explain the results obtained in different tissues but also help to understand the difference between estimating the parallel or the perpendicular AxTM. After that, our main findings are stated and the corresponding results are reported (Section 3.2).

3.1 | Diffusion signal profiles influenced by fiber alignment

Each of the simulated voxels of the `synthetic dataset` shows a characteristic, ψ dependent shape, see Figure 5. For smaller angles ψ between $\psi = 10°$ and $\psi = 0°$, the simulated signals of the HA voxel are strongly diffusion weighted and are close or below the noise floor (SNR = 1), see Figure 5A. In the simulated voxel of MA, the noise floor is already reached for angles $\psi \approx 50°$, see Figure 5B. In the simulated LA voxel the noise floor is never reached and the simulation shows a seemingly constant, ψ independent signal form, see Figure 5C. In summary, the signal in HA to MA decays along the direction of symmetry, whereas there is almost no decay in LA.

3.2 | Results of simulation study

Figure 6 shows the SNRs required to accurately estimate the AxTM (A-MPE < 5%, Equation 8) in the `synthetic` and `in-vivo white matter dataset`. Shown are

the results for axisymmetric DKI and standard DKI with (hatched) or without RBC.

3.2.1 | RBC is most effective in highly aligned fibers and parallel diffusion case

RBC was most effective for the parallel parameters $D_{\parallel}$ and $W_{\parallel}$ in HA to MA (for both the synthetic and `invivo white matter dataset`), see Figure 6. For example, achieving A-MPE <5% for $W_{\parallel}$ in the synthetic HA voxel could be reduced from SNR = 81 to SNR = 25 (standard DKI) or SNR = 29 (axisymmetric DKI). In the in-vivo white matter voxels, the SNR requirements for achieving A-MPE <5% for $W_{\parallel}$ could be reduced from 20 to 10 (standard DKI) or to 8 (axisymmetric DKI). Estimation of $\overline{W}$ was significantly improved by RBC in the synthetic HA and MA voxels but only slightly in the `in-vivo white matter datasets`.

3.2.2 | Superiority of axisymmetric DKI in axisymmetric fibers with low alignment where RBC is ineffective

In the synthetic LA voxel, estimation of $D_{\parallel}$, $D_{\perp}$, $W_{\parallel}$, and $W_{\perp}$ was substantially improved by using the axisymmetric DKI framework instead of standard DKI. For example, it only required an SNR = 15 (axisymmetric DKI) instead of SNR = 51 (standard DKI) to achieve A-MPE <5% for
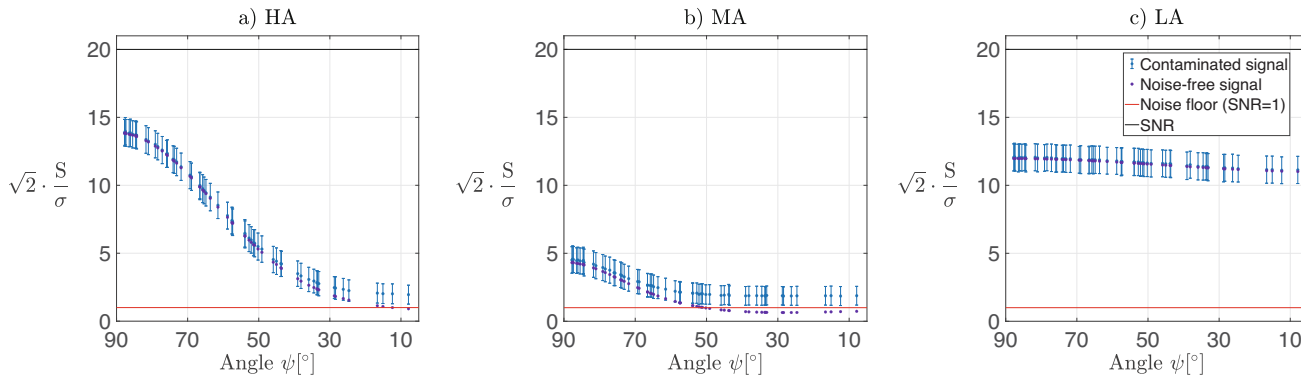
FIGURE 5 Simulated signal decay along the axis of symmetry at signal-to-noise ratio (SNR) = $\sqrt{2}S_0/ = 20$. Signal decay is shown for the `synthetic dataset` consisting of A) highly aligned fibers (HA), B) fibers with moderate alignment (MA) and C) fibers with low alignment (LA) as a function of angle ψ between the diffusion gradient $\vec{g}$ and the axis of symmetry $\vec{c}$, see Section 2.5. The "Contaminated signal" shows the mean and SD over 2500 noise-samples. Plotted is the quantity $\sqrt{2} \cdot S/\sigma$, which is the SNR computed for the diffusion weighted signal S (instead of S_0) at a given angle ψ (for a graphical representation of angle ψ see Figure 4). The red horizontal line indicates the noise floor where SNR = 1. All three plots were calculated for the highest b-shell (b = 2500 s/mm^2).
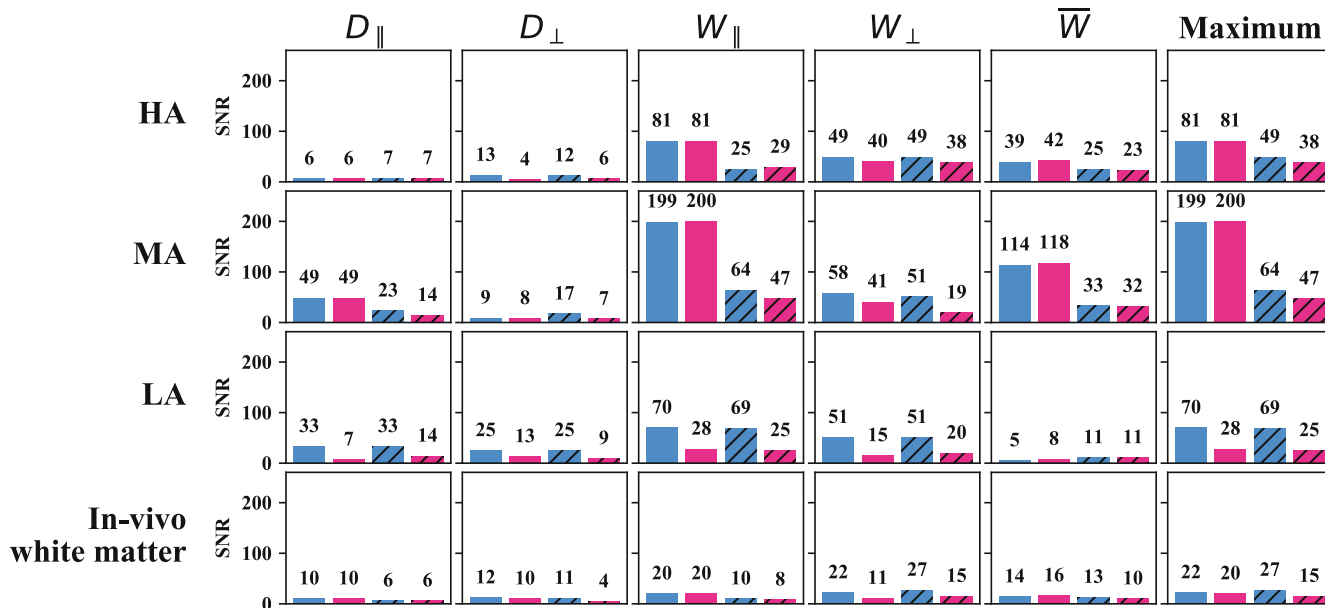

FIGURE 6 Signal-to-noise ratio (SNR) above which the absolute value of the mean percentage error (A-MPE, Equation 8) < 5% for the `synthetic dataset` with high, medium and low fiber alignment ("HA", "MA," "LA") and the `in-vivo white matter dataset`. For the `in-vivo white matter dataset`, the A-MPE was averaged across the 12 simulated voxels and the SNR above which this average A-MPE < 5% is shown. The SD across the in-vivo white matter dataset voxels is not shown here because the values were between ≈ 0.5 and ≈ 6 with an average of ≈ 2.5 and thus to small to display. The number above the barplots indicates the barplot's height. Blue encodes standard DKI, red encodes axisymmetric DKI, the hatched barplots show the results if RBC is used. "Maximum" shows the maximum SNR needed to achieve A-MPE < 5% across all five AxTM.

$W_\perp$. For $\overline{W}$, axisymmetric DKI performed slightly worse than standard DKI (SNR = 8 instead of SNR = 5). Interestingly, RBC did not influence the fitting results much in this fiber alignment configuration but even worsened them in some cases (e.g., axisymmetric DKI results for $D_\parallel$), see Figure 6.

3.2.3 | Axisymmetric DKI improves estimation of perpendicular parameters

Estimation of $D_\perp$ and $W_\perp$ could also be improved (A-MPE < 5% reached for lower SNRs) by using the axisymmetric DKI framework in HA and MA of the `synthetic`

and `in-vivo white matter dataset` (e.g., for HA, $D_\perp$: SNR = 4 instead of SNR = 13; $W_\perp$: SNR = 40 instead of SNR = 49).

3.2.4 | RBC can also worsen accuracy

Interestingly, there were also few scenarios in which RBC increased the SNR requirements. As described above this was observed for $D_\parallel$, $W_\perp$, and $\overline{W}$ in the LA voxel and, outside the LA voxel, predominantly for the perpendicular parameters, for example, from SNR = 11 to SNR = 15 for the axisymmetric DKI fit of $W_\perp$ in the `in-vivo white matter dataset`.

4 | DISCUSSION

4.1 | Summary of main findings

Overall, we found, that the combination of axisymmetric DKI with RBC was the best option for estimating all five AxTM in the `synthetic` and `in-vivo white matter` datasets, see "Maximum" column of Figure 6. This combination achieved an absolute value of the mean percentage error (A-MPE, Equation 8) < 5% in our simulated `in-vivo white matter data` if the SNR ≥ 15, making this combination a possibly valuable tool in neuroscience and clinical research studies focusing on white matter. Specifically, we found that RBC is highly effective for increasing estimation accuracy of the AxTM associated with diffusion parallel to the main fiber orientation, that is, parallel diffusivity and kurtosis, in in-vivo white matter. In contrast, RBC fails in improving estimation accuracy in parameters perpendicular to the main fiber orientation, that is, perpendicular diffusivity and kurtosis, or if fiber alignment is too low. For the latter scenarios, axisymmetric DKI is more effective than standard DKI in in-vivo white matter or the synthetic LA voxel.

4.2 | Rician noise bias and its correction: Effectiveness for different DKI parameters and levels of fiber alignment within white matter

The effectiveness of RBC correlated with the severity of the Rician noise bias, it varied between individual AxTM and depended on the level of fiber alignment. The severity of the Rician noise bias is inversely proportional to the SNR which in turn depends on a variety of parameters. One of these parameters is the level of water mobility which tunes the diffusivity and thereby the attenuation of the diffusion weighted signal. Water mobility is influenced by the level of fiber alignment. Furthermore, each AxTM itself is associated with different levels of water mobility due to its association to the axis of symmetry $\vec{c}$. Figure 5 shows simulated signals in three tissue types with varying degrees of fiber alignment as a function of angle ψ between $\vec{c}$ and diffusion gradient $\vec{g}$. In HA for example, the diffusion signal is heavily diffusion weighted if measured along the main fiber orientation (small angle ψ) and the Rician noise bias in these signals therefore strongest, see Figure 5A. Since the parallel AxTM ($D_\parallel$ and $W_\parallel$) predominantly depend on the signal along these directions, it can be expected that they, too, are more heavily biased in a high fiber alignment setting. Accordingly, we found that RBC turned out to be particularly important for the AxTM associated with parallel diffusion ($D_\parallel$ and $W_\parallel$) in highly aligned white matter (`synthetic dataset` and `in-vivo white matter dataset`). On the other hand, diffusion perpendicular to $\vec{c}$ will be more restricted than the parallel diffusion and the SNR therefore higher along those directions. $D_\perp$ and $W_\perp$ should therefore be less affected by the Rician noise bias. Indeed, we found that RBC was not as effective for the perpendicular parameters $D_\perp$ and $W_\perp$ in in-vivo white matter and HA as for the parallel parameters. An apparent contradiction to this argument was found for $W_\perp$ in the synthetic MA dataset. This contradictory finding, however, can be explained by the relatively high perpendicular diffusivity of the MA voxel (Table S1 of Appendix S1) causing a strong diffusion weighting and therefore smaller perpendicular signal in this case (Figure 5B).

RBC was furthermore ineffective in the synthetic LA voxel, see Figure 6. Here, the signal change as a function of angle ψ between $\vec{c}$ and $\vec{g}$ is smaller than the variation introduced by noise and the signals almost seem independent of the diffusion gradient direction, see Figure 5C. This is because the synthetic LA voxel does not posses a clearly distinguishable axis along which water mobility is significantly heightened compared to other directions. For the same SNR (in reference to the S_0 signal), the Rician noise bias in such tissues is therefore less severe, compared to, for example, signals in HA acquired for diffusion gradients parallel to the axis of symmetry. Accordingly, we found that RBC had little to no effect on parameter estimation in the synthetic LA voxel. In addition to this, the original, seemingly constant signal pattern could be modified by the noise in such a way that the RBC might even worsen the bias if it acts on the noisy signals and further shifts them away from their original, seemingly constant pattern. For example, signals that were reduced due to noise might be further reduced by the RBC.

4.3 | Advantage of the axisymmetric DKI framework

In Section 1, we hypothesized that a reduction of the parameter space could make axisymmetric DKI more robust against the Rician noise bias. We observed that axisymmetric DKI predominantly improved accuracy of parameter estimation of the perpendicular AxTM $D_\perp$ and $W_\perp$ in both the `synthetic dataset` (HA and MA voxels) and the `in-vivo white matter dataset`, that is, A-MPE < 5% was achieved for lower SNRs when using axisymmetric DKI to estimate these metrics.

The increased accuracy for $W_\perp$ when using the axisymmetric DKI framework can be understood with the information provided in Reference 3. Here an approach for estimation of $W_\perp$ (equation 24 in Reference 3) with the axisymmetric DKI framework is outlined that only depends on measurements with diffusion gradients perpendicular to the principal diffusion axis (axis of symmetry $\vec{c}$) and the square of the MD. The measurements perpendicular to the main diffusion axis are less strongly attenuated because diffusivity is lower in that direction, see Section 4.2. Therefore, these signals are less strongly affected by the Rician bias. Moreover the MD, which depends on diffusion gradients that are not perpendicular to the principal diffusion axis, can be estimated from the lower diffusion shells in a DKI acquisition. Thus, the influence of the Rician bias on the MD is lower. Taken together, the estimation of $W_\perp$ with axisymmetric DKI can be done based on "perpendicular measurements" (for the higher b-shell) and the MD which are both less strongly affected by the Rician noise bias resulting in a reduced bias of $W_\perp$. The observed improvement for $D_\perp$ can be understood following the same line of thought and equation 23 in Reference 3 which lays out a scheme for estimating $D_\perp$ based on axisymmetric DKI and measurements with diffusion gradients perpendicular to the principal diffusion axis.

Another observation was that, accuracy of parameter estimation with axisymmetric DKI was substantially better in tissues with low fiber alignment (Figure 6) compared to standard DKI. We observed, for example, an SNR reduction of up to 70% when using axisymmetric DKI instead of standard DKI for estimation of $W_\perp$ in the LA voxel, see Figure 6. This could be due to the seemingly constant and high signal, independent of the diffusion gradient direction, in the synthetic LA dataset. Since the variation in the almost constant diffusion signal is dominated by noise, the complex 22 parametric standard DKI framework is more likely to overfit the data than the eight parametric axisymmetric DKI framework, particularly in case of lower SNRs where noise has a greater impact. This could be the reason for the clear advantage of axisymmetric DKI over standard DKI in this fiber configuration. However, axisymmetry in the underlying fibers could be a crucial prerequisite for observing this improvement in LA-type voxels using axisymmetric DKI, see Section 4.4.

4.4 | Extra analyses and considerations

4.4.1 | In-vivo gray matter simulation

In comparison to white matter, gray matter does not possess a clear axis of symmetry which makes it less suitable for axisymmetric DKI.[3] However, in practice axisymmetric DKI metrics can generally also be computed in gray matter which is why we also simulated and analyzed axisymmetric DKI in in-vivo gray matter, see Section S1.5 and Figure S1 of Appendix S1. Gray matter could potentially be modeled by the synthetic voxel of fibers with low alignment (LA) shown in Figure 4. Comparing the SNR needed by each fitting method to reach the A-MPE < 5% threshold in in-vivo gray matter with the synthetic LA configuration (Figure 6, main document or Figure S1 of Appendix S1) revealed that axisymmetric DKI is performing better than standard DKI in the synthetic LA voxel but worse in the in-vivo gray matter dataset.

An intuitive explanation for the observed deviation could be that violation of the assumption of axisymmetry in gray matter leads to an inherent bias of the axisymmetric DKI parameter estimates that cannot be neglected. This intuitive explanation is further supported by our recent study[31] where we experimentally observed a deviation between standard DKI and axisymmetric DKI parameter estimates in the brain. However, this intuitive explanation would be in contradiction to a recently introduced analytical proof[32] showing that axisymmetric DKI and standard DKI produce the same parameter estimates even if axisymmetry in the underlying tissue is not fulfilled. However, this proof only holds under the condition that the first eigenvector of the diffusion tensor aligns with the axis of symmetry. Therefore, a thorough analysis is required in future studies to improve our understanding of the observed deviations between the analytical proof and the experimental observations.

4.4.2 | Analysis of precision

We have additionally investigated the precision of the four proposed methods for in-vivo white matter by calculating the SD in reference to the ground truth (R-STD) of each method (see Section S1.6 of Appendix S1). Our main findings were: first, the precision was not improved by RBC. Second, the precision of axisymmetric DKI was

worse than that of standard DKI. The first finding was expected because RBC does not improve precision. RBC shifts the expectation value (modeled by the mean) of the distribution of fit results toward the ground truth; however, this does not influence the width of the distribution of fit results which defines the precision by which a quantity can be estimated. Improvement of precision can be achieved by either averaging multiple identically performed measurements or by applying de-noising methods like, for example, done in Reference 14. Our second finding is in contrast to what we have assumed in the introduction of our article, namely that axisymmetric DKI is less susceptible to the noise-induced variation of the acquired diffusion MRI signals compared to standard DKI due to its smaller parameter space. Our findings show that the SNR required to reach the R-STD $\leq$ 5% threshold was typically slightly and in some cases substantially (e.g., `in-vivo white matter dataset` for $W_\perp$) higher when using axisymmetric DKI compared to standard DKI. The case of substantially higher SNRs required to reach the R-STD $\leq$ 5% threshold in the axisymmetric DKI fit results could be connected to outliers. The interquartile range was used to compute a robust, that is, less outlier sensitive, measure ("R-IQR") for the SD, see Section S1.6 of Appendix S1. With respect to the R-IQR, standard DKI, and axisymmetric DKI performed almost identically in in-vivo white matter for $W_\perp$, making the outliers in axisymmetric DKI a highly likely explanation for the stark difference in precision between standard and axisymmetric DKI in this case. However, even when using the outlier-robust R-IQR measure, both DKI frameworks perform very similar, that is, axisymmetric DKI seems to not have an improved precision (compared to standard DKI) despite its smaller parameter space. One reason that might explain this finding could be that the axisymmetric DKI framework cannot be linearised (in contrast to standard DKI) and thus might be more susceptible to noise, for example, due to noise enhancement.

4.4.3 | Error propagation in standard DKI

The five AxTM can be calculated from the standard DKI tensor metrics. The number of standard DKI metrics needed to compute each AxTM is listed in Table 1. This property illustrates the risk of error propagation of the base standard DKI tensor metrics into the AxTM. The uncertainty of each estimated standard DKI metric propagates into the resulting AxTM computed from them resulting in a dependency of the uncertainty on the number of the base standard DKI tensor metrics. $D_\parallel$, for example, relies on only one parameter while $W_\perp$ relies on three, so that a

priori it can be assumed that $W_\perp$ is more severely affected by uncertainty propagation in standard DKI.

4.4.4 | Possible circularity of simulation study

Since the simulation studies were either based on the axisymmetric DKI (`synthetic dataset`) or the standard DKI framework (`in-vivo white matter dataset`), one might argue that the simulations will favor their respective signal frameworks. Here we rediscuss our signal-framework comparisons in the light of this potential circularity: We observed that using axisymmetric DKI was generally advantageous over standard DKI for the perpendicular AxTM. Axisymmetric DKI was also performing significantly better on all AxTM except $\overline{W}$ in the LA dataset. Since the improvement of axisymmetric DKI over standard DKI for the perpendicular AxTM was observed across both simulations, the observation cannot be explained by a circularity argument and we believe that it is a genuine advantage of axisymmetric DKI. The have additionally investigated the synthetic LA dataset, however, is based on the axisymmetric DKI framework and the better results might well be confounded by the circularity argument. However, our noise-robustness argument is also a reasonable explanation for the superiority of axisymmetric DKI in this case. Thus, the truth might be in between, that is, the real improvement of estimation accuracy in the LA dataset when using axisymmetric DKI might be lower than in the simulation but we would expect to still observe an improvement in in-vivo data given a sufficient level of axisymmetry.

4.4.5 | Limits of current measurements protocols

Looking at the estimation accuracy for each of the five AxTM individually revealed that each metric comes with different SNR requirements. Estimation of $W_\parallel$ with an A-MPE <5%, for example, required an SNR of 81 in the HA voxel of the `synthetic dataset` and an SNR of 199 (standard DKI) or 200 (axisymmetric DKI) in the MA voxel of the `synthetic dataset` if RBC was not used. This reveals that using current measurement protocols could yield biased estimates under realistic conditions where the SNR is below 81 or 200 if RBC is not used. This underlines the importance of using RBC in cases where all five AxTM are of importance, for example, for estimation of the biophysical microstructure parameters.[18,19]

4.4.6 | Limits of RBC for single voxel application

Similar to previous simulation studies on RBC,[10,13,14] we focused on the effects of RBC on the averaged estimated AxTM over the 2500 noise samples which is a stable estimator for the expectation value of the distribution of the fit results. The SNR at which that expectation value of the AxTM could be estimated with an A-MPE < 5% is reported in this article. If this expectation value is unbiased for a specific SNR, the underlying DKI framework is demonstrated to be unbiased, as well. Parameter estimation based on real, in-vivo measurements typically relies on only one noise realization. Therefore, the SNR results from our simulation study cannot be transferred directly to standard in-vivo DWI measurements. The SNRs found in our simulation study show when the estimator itself is unbiased given sufficient repetitions. We also investigated the SNR requirements for a high precision and found that much higher SNRs were required (see Section S1.6 of Appendix S1 or Section 4.4.2 above for a more general discussion of estimation precision).

5 | CONCLUSION

Our study revealed that axisymmetric DKI with RBC is the most SNR effective choice for estimating the AxTM in tissues that do not violate its assumptions because of two mutually supporting factors. First, RBC itself is most effective for the parallel diffusivity and kurtosis and the mean of the kurtosis tensor, however, it needs at least some level of fiber alignment to work. Second, compared to standard DKI, axisymmetric DKI is superior in axisymmetric fibers with low alignment and more effective for estimating the perpendicular diffusivity and kurtosis. This makes the combination of axisymmetric DKI with RBC a possibly valuable tool for neuroscience and clinical research studies focusing on white matter where a gain in SNR could either be used to reduce scan time or increase spatial resolution.

AUTHORS' CONTRIBUTIONS
Jan Malte Oeschger: Conceptualization, Data curation, Formal analysis, Investigation, Methodology, Software, Visualization, Writing – original draft, **Karsten Tabelow:** Conceptualization, Methodology, Supervision, Writing – review ς editing, **Siawoosh Mohammadi:** Conceptualization, Funding acquisition, Methodology, Project administration, Resources, Supervision, Writing – review & editing.

DATA AVAILABILITY STATEMENT
The open-source ACID toolbox (http://www.diffusiontools.com/) for SPM contains the fitting algorithms for standard and axisymmetric DKI with and without RBC used in this study. Furthermore, a code repository for simulation and analysis of the data used in this study will be made available at https://github.com/quantitative-mri-and-in-vivo-histology/axisymmetric_dki_with_rician_bias_correction_simulation_study.

ETHICS STATEMENT
The in-vivo dMRI data used for this study were acquired with the help of a human research participant. The participant provided written informed consent and was compensated for its participation. The local ethics committees at University Medical Center Hamburg-Eppendorf approved the study (PV5141).

ORCID
Jan Malte Oeschger https://orcid.org/0000-0003-0237-923X
Karsten Tabelow https://orcid.org/0000-0003-1274-9951
Siawoosh Mohammadi https://orcid.org/0000-0003-1311-9636

REFERENCES

1. Deppe M, Kellinghaus C, Duning T, et al. Nerve fiber impairment of anterior thalamocortical circuitry in juvenile myoclonic epilepsy. *Neurology*. 2008;71:1981-1985.

2. Rovira À, Wattjes MP, Tintoré M, et al. MAGNIMS consensus guidelines on the use of MRI in multiple sclerosis—Clinical implementation in the diagnostic process. *Nat Rev Neurol*. 2015;11:471-482.

3. Hansen B, Shemesh N, Jespersen SN. Fast imaging of mean, axial and radial diffusion kurtosis. *NeuroImage*. 2016;142:381-393.

4. Hansen B, Jespersen SN. Recent developments in fast kurtosis imaging. *Front Phys*. 2017;5:40.

5. Jensen JH, Helpern JA, Ramani A, Lu H, Kaczynski K. Diffusional kurtosis imaging: the quantification of non-Gaussian water diffusion by means of magnetic resonance imaging. *Magn Reson Med*. 2005;53:1432-1440.

6. Derek P, Jones K. *Diffusion MRI Theory, Methods, and Applications: Theory, Methods, and Applications*. Oxford University Press; 2012.

7. Henkelman RM. Measurement of signal intensities in the presence of noise in MR images. *Med Phys*. 1985;12:232-233.

8. Gudbjartsson H, Patz S. The Rician distribution of noisy MRI data. *Magn Reson Med*. 1995;34:910-914.

9. Sijbers J, den Dekker A, Scheunders P, Van Dyck D. Maximum-likelihood estimation of Rician distribution parameters. *IEEE Trans Med Imaging*. 1998;17:357-361.

10. Veraart J, Rajan J, Peeters RR, Leemans A, Sunaert S, Sijbers J. Comprehensive framework for accurate diffusion MRI parameter estimation. *Magn Reson Med*. 2013;70:972-984.

11. Glenn GR, Tabesh A, Jensen JH. A simple noise correction scheme for diffusional kurtosis imaging. *Magn Reson Imaging*. 2015;33:124-133.

12. Koay CG, Özarslan E, Basser PJ. A signal-transformational framework for breaking the noise floor and its applications in MRI. *J Magn Reson*. 2009;197:108-119.

13. Veraart J, Hecke WV, Sijbers J. Constrained maximum likelihood estimation of the diffusion kurtosis tensor using a Rician noise model. *Magn Reson Med*. 2011;66:678-686.

14. André ED, Grinberg F, Farrher E, et al. Influence of noise correction on intra- and inter-subject variability of quantitative metrics in diffusion kurtosis imaging. *PLoS One*. 2014;9:e94531.

15. Coutu J-P, Chen JJ, Rosas HD, Salat DH. Non-Gaussian water diffusion in aging white matter. *Neurobiol Aging*. 2014;35:1412-1421.

16. Genç E, Fraenz C, Schlüter C, et al. Diffusion markers of dendritic density and arborization in gray matter predict differences in intelligence. *Nat Commun*. 2018;9:1-11.

17. Donat CK, Yanez Lopez M, Sastre M, et al. From biomechanics to pathology: predicting axonal injury from patterns of strain after traumatic brain injury. *Brain*. 2021;144:70-91.

18. Novikov DS, Veraart J, Jelescu IO, Fieremans E. Rotationally-invariant mapping of scalar and orientational metrics of neuronal microstructure with diffusion MRI. *NeuroImage*. 2018;174:518-538.

19. Jespersen SN, Olesen JL, Hansen B, Shemesh N. Diffusion time dependence of microstructural parameters in fixed spinal cord. *NeuroImage*. 2018;182:329-342.

20. Jensen JH, Helpern JA. Quantifying non-Gaussian water diffusion by means of pulsed-field-gradient MRI. Proceedings of ISMRM 2003; 2003:2154.

21. Hansen B, Lund TE, Sangill R, Jespersen SN. Experimentally and computationally fast method for estimation of a mean kurtosis. *Magn Reson Med*. 2013;69:1754-1760.

22. Hansen B, Khan AR, Shemesh N, et al. White matter biomarkers from fast protocols using axially symmetric diffusion kurtosis imaging. *NMR Biomed*. 2017;30:e3741.

23. Tabesh A, Jensen JH, Ardekani BA, Helpern JA. Estimation of tensors and tensor-derived measures in diffusional kurtosis imaging. *Magn Reson Med*. 2011;65:823-836.

24. Veraart J, Sijbers J, Sunaert S, Leemans A, Jeurissen B. Weighted linear least squares estimation of diffusion MRI parameters: strengths, limitations, and pitfalls. *NeuroImage*. 2013;81:335-346.

25. Mohammadi S, Tabelow K, Ruthotto L, Feiweier T, Polzehl J, Weiskopf N. High-resolution diffusion kurtosis imaging at 3T enabled by advanced post-processing. *Front Neurosci*. 2015;8:1-14.

26. Polzehl J, Tabelow K. Low SNR in diffusion MRI models. *J Am Stat Assoc*. 2016;111:1480-1490.

27. Modersitzki J. *FAIR: Flexible Algorithms for Image Registration*. SIAM; 2009.

28. Coelho S, Pozo JM, Jespersen SN, Jones DK, Frangi AF. Resolving degeneracy in diffusion MRI biophysical model parameter estimation using double diffusion encoding. *Magn Reson Med*. 2019;82:395-410.

29. Benitez A, Fieremans E, Jensen JH, et al. White matter tract integrity metrics reflect the vulnerability of late-myelinating tracts in Alzheimer's disease. *NeuroImage Clini*. 2013;4:64-71.

30. Eickhoff SB, Stephan KE, Mohlberg H, et al. A new SPM toolbox for combining probabilistic cytoarchitectonic maps and functional imaging data. *NeuroImage*. 2005;25:1325-1335.

31. Oeschger JM, Tabelow K, Mohammadi S. Violation of axial-symmetric assumption in DKI and consequences for biophysical parameter estimates across white matter. Proceedings of ISMRM 2022; 2022:0982.

32. Nørhøj Jespersen S. White matter biomarkers from diffusion MRI. *J Magn Reson*. 2018;291:127-140.

SUPPORTING INFORMATION

Additional supporting information may be found in the online version of the article at the publisher's website.

Appendix S1. Supporting information